



Anisotropic Deformation in Refractory Multi-principal Element Alloys: Insights from Atomistic Simulations and Machine Learning

Abdullah Al Mamun¹ · Xiang-Guo Li² · Shuzhi Xu³ · Yanqing Su¹

Received: 17 December 2024 / Accepted: 20 March 2025 / Published online: 4 April 2025
© The Author(s) 2025

Abstract

Refractory multi-principal element alloys (RMPEAs) represent an advanced subclass of MPEAs, distinguished by their complex multi-element compositions and significant inclusion of refractory elements. This study investigates the mechanical behavior of RMPEAs under compressive and tensile loading using molecular dynamics (MD) and hybrid MD/Monte Carlo (MD/MC) simulations. Mechanical responses are analyzed across a broad temperature range (300 K to 1673 K) for 16 alloy configurations, comprising one quinary, five quaternaries, and ten ternaries in post-MD/MC equilibrated states. A particular emphasis is placed on the roles of chemical short-range order and lattice distortion in influencing anisotropic mechanical properties. Compressive yield stresses are consistently higher than tensile yield stresses across all temperatures and compositions, demonstrating plastic anisotropy. Machine learning (ML) models reveal that temperature, lattice distortion, and Warren–Cowley parameter (WCP) values for pairs like Ta-Ta and Nb-Ta, and concentrations of Mo, W, and Nb are the most significant factors influencing yield stresses. Additionally, the ML models identify atomic size mismatch as the dominant contributor to lattice distortion, with WCP values playing a secondary role. The study also uncovers that while the lattice distortion promotes plastic anisotropy, the chemical short-range order decreases it, highlighting the critical interplay between atomic structure and mechanical behavior in RMPEAs.

Keywords Refractory multi-principal element alloys · Chemical short-range order · Lattice distortion · Yield stress · Machine learning · Anisotropy

Introduction

Refractory multi-principal element alloys (RMPEAs) belong to a specialized subset of MPEAs, primarily formulated from refractory metals such as Mo, Ti, V, Nb, Hf, Ta, Cr, and W. Two of the pioneering RMPEAs, MoNbTaW and MoNbTaVW, were first introduced by Senkov et al. in 2010 [1]. The research team conducted comprehensive examinations of the lattice parameters, crystal structure, and mechanical attributes of these systems. Their findings revealed that these

alloys exhibited a simple body-centered cubic (BCC) crystal structure. Remarkably, the Vickers hardness values for these alloys exceeded theoretical predictions derived from the rule of mixtures by a factor of 2 to 3. In addition, the alloys retained significant strength at temperatures up to 1600 °C, with yield stress (normalized by density) 2 to 4 times higher than that of Inconel 718 and Haynes 230 at 1273 K [2].

Further studies explore many other RMPEAs. The mechanical properties of RMPEAs are influenced by their unique structural characteristics, particularly lattice distortion and chemical short-range order (CSRO) [3]. In these alloys, where multiple principal elements coexist in a solid solution phase, each atom deviates from its average lattice position due to neighboring atoms with varying atomic sizes. This severe lattice distortion has been correlated with enhanced yield strengths and high hardness, as it introduces significant resistance to dislocation motion [4–6]. The presence of CSRO, a non-random arrangement of atoms within the solid solution, plays a critical role in modifying the microstructural characteristics that influence mechanical

✉ Yanqing Su
yanqing.su@usu.edu

¹ Department of Mechanical and Aerospace Engineering, Utah State University, Logan, UT 84322-4130, USA

² School of Materials, Shenzhen Campus of Sun Yat-sen University, Shenzhen 518107, Guangdong, People's Republic of China

³ School of Aerospace and Mechanical Engineering, University of Oklahoma, Norman, OK 73019-1052, USA

behavior. CSRO affects basic structural parameters [7], stacking-fault energy [8], shear strength [9], and dislocation mobility [10, 11], all of which contribute to the exceptional mechanical properties observed in these alloys. Additionally, RMPEAs with a single-phase BCC structure show outstanding resilience to challenges like void swelling, irradiation-induced segregation, and hardening, indicating their potential for advanced applications in extreme environments [12–14]. These attributes make RMPEAs very suitable for use in demanding environments, where high-temperature strength and stability are critical, such as aircraft engines and nuclear reactors [15]. The combination of high hardness, significant yield strength retention at elevated temperatures, and resilience against radiation damage makes RMPEAs a promising material class for future high-performance applications [16–18].

Atomistic simulations serve as a robust adjunct to theoretical analyses and expensive experiments [19]. The exploration of RMPEAs using atomistic simulations is crucial for understanding and predicting their properties because the atomic-level structure significantly influences the anisotropic properties of these alloys [20], such as tensile and compressive yield stress, adding complexity to experimental materials characterization [21]. The accuracy of atomistic simulations primarily relies on the quality of interatomic potentials [22]. Liu et al. [23] investigated the mechanical properties of AlCrCuFeNi MPEA under uniaxial tensile load, revealing not only high strength but also appreciable ductility. The plastic deformation of the alloy was primarily attributed to dislocation glide, lattice distortion, and twinning mechanisms during tensile testing. Qi et al. [24] focused on the plastic deformation of single-crystal and polycrystalline CoCrFeMnNi MPEA under tensile and compressive stresses using atomistic simulations.

Several recent studies have reported on the accuracy and efficiency of machine learning (ML)-based interatomic potentials in comparison to density functional theory (DFT) results [25, 26]. For instance, Byggmäster et al. [27] trained a Gaussian approximation potential (GAP) to investigate defects in the MoNbTaVW RMPEA. Wang et al. [3] recently trained a moment tensor potential (MTP) to reveal the influence of lattice distortion and CSRO on the dislocation mechanism in the MoNbTaVW alloy. More recently, Mubassira et al. [28] utilized the MTP to analyze the effect of CSRO on lattice parameter and unstable stacking-fault energy of several RMPEAs.

However, a systematic investigation of CSRO from elevated to room temperature and its effect on mechanical properties, particularly how these properties change with temperature variation, has yet to be thoroughly studied. Xu et al. [21] investigated the mechanical anisotropy of nanowires in 16 RMPEAs, finding that they exhibit reduced tension–compression asymmetry compared to pure metals.

A similar conclusion was reached by Pan et al. [29] who used an ML-based spectral neighbor analysis potential to study the MoNbTaW MPEA. Both pieces of work pointed that the underlying deformation mechanism for compression is dislocation slip while that for tension is twinning. Nevertheless, only random atomistic structures at a single temperature were considered in each study. The effects of CSRO and temperature are yet to be addressed.

To address this gap, the present study systematically investigates the anisotropic properties, including both the compressive and tensile yield stress and their ratio, and the effect of lattice distortion, CSRO, and temperature. Utilizing using molecular dynamics (MD) and hybrid MD/ Monte Carlo (MD/MC) simulations, this research seeks to provide a comprehensive understanding of the mechanical behavior of the Mo–Nb–Ta–V–W alloy system and its subsets. Five temperatures are considered: 300 K, 573 K, 873 K, 1373 K, and 1673 K. 16 different alloy compositions are explored, ranging from quinary to ternary systems, in equilibrated states obtained by hybrid MD/MC simulations. A critical aspect of this investigation is to understand the effects of CSRO and lattice distortion on the anisotropic properties of RMPEAs. In addition, three ML models are trained to identify the key features that influence compressive stress, tensile stress, and the ratio of compressive to tensile stress. This comprehensive approach seeks to advance the understanding of the mechanical properties of RMPEAs, contributing to the development of high-performance materials for extreme environments.

Methods

Moment Tensor Potential

We utilize the ML-based MTP recently developed by Wang et al. [3] for the alloy system comprised of Mo, Nb, Ta, V, and W. The MTP lies in the concept of interatomic pairwise potential energy moments. It employs contracted rotationally invariant descriptors of the local environment around each atom. These descriptors are then utilized to establish a polynomial regression that correlates the potential energy surface with these local environment descriptors [30]. All alloys studied here are summarized in Table 1.

Validation and Transferability of the MTP

The MTP [3] used in this study was trained on a diverse dataset to ensure robustness across various atomic environments. The training set includes pure metals, binaries, ternaries, quaternaries, and a quinary within the Mo–Nb–Ta–V–W system, with configurations obtained from *ab initio* MD simulations at 300 K, 1000 K, and 3000

Table 1 16 RMPEAs studied in this work

Compositions	
Quinary	MoNbTaVW
Quaternary	MoNbTaW, MoNbVW, MoTaVW, NbTaVW, MoNbTaV
Ternary	MoNbW, MoTaW, MoVW, NbTaW, NbVW, TaVW, NbTaW, MoNbV, MoTaV, NbTaV

K, respectively. Particularly, the high-temperature configurations, e.g., 3000 K that is above the melting points, can preserve a high extent of distortion. Additionally, strained structures with deformations ranging from -10% to $+10\%$ were incorporated, ensuring the potential's applicability to high-strain conditions. This training dataset captures CSRO effects and strain variations, making the potential well suited for modeling stress–strain responses and mechanical behavior in RMPEAs. The potential was benchmarked against DFT calculations, achieving a mean absolute error of less than 3 meV/atom for energy and below 0.05 eV/ \AA for force, demonstrating its high accuracy in predicting structural and mechanical properties. Lattice constants and elastic constants were obtained using this potential, with bulk modulus, shear modulus, and Poisson's ratio derived from them, demonstrating excellent agreement with DFT values.

Hybrid MD/MC simulation

All atomistic simulations in this paper are conducted using LAMMPS [31]. Initially, a simulation cell measuring

$6.4\text{nm} \times 6.4\text{nm} \times 9.6\text{nm}$ is constructed. This cell is oriented with the crystallographic directions [100], [010], and [001] aligned along the x , y , and z axes, respectively. Periodic boundary conditions (PBCs) are applied in all three directions. The simulation cell is populated with 24,000 atoms, and the solute types are initially randomly distributed within the cell to achieve the target concentration of the simulated alloy. Subsequently, hybrid MD/MC simulations are utilized to obtain structures containing CSRO, at annealing temperatures of 300 K, 573 K, 873 K, 1373 K, and 1673 K, respectively, using the NPT ensemble. During each MC step, pairs of atoms are swapped for each of the defined type combinations, and this process is repeated until the system converges, as indicated by a reduction in the potential energy per atom. The decrease in potential energy until it becomes a flat line for the MoNbVW, MoNbTaW, and MoNbW alloys is shown in Fig. 1.

Warren–Cowley Parameter

Warren–Cowley parameters (WCP) measure the degree of CSRO [32]. For like atoms, positive values mean they prefer to be neighbors. For unlike atoms, negative WCP values show a preference for pairing. The 1st nearest neighbor WCP is formulated as [33]

$$\alpha_{ij} = \frac{p_{ij} - c_j}{\delta_{ij} - c_j}, \quad (1)$$

where p_{ij} denotes the probability of a j -type atom being around an atom of type i within the 1st shell, c_j is the

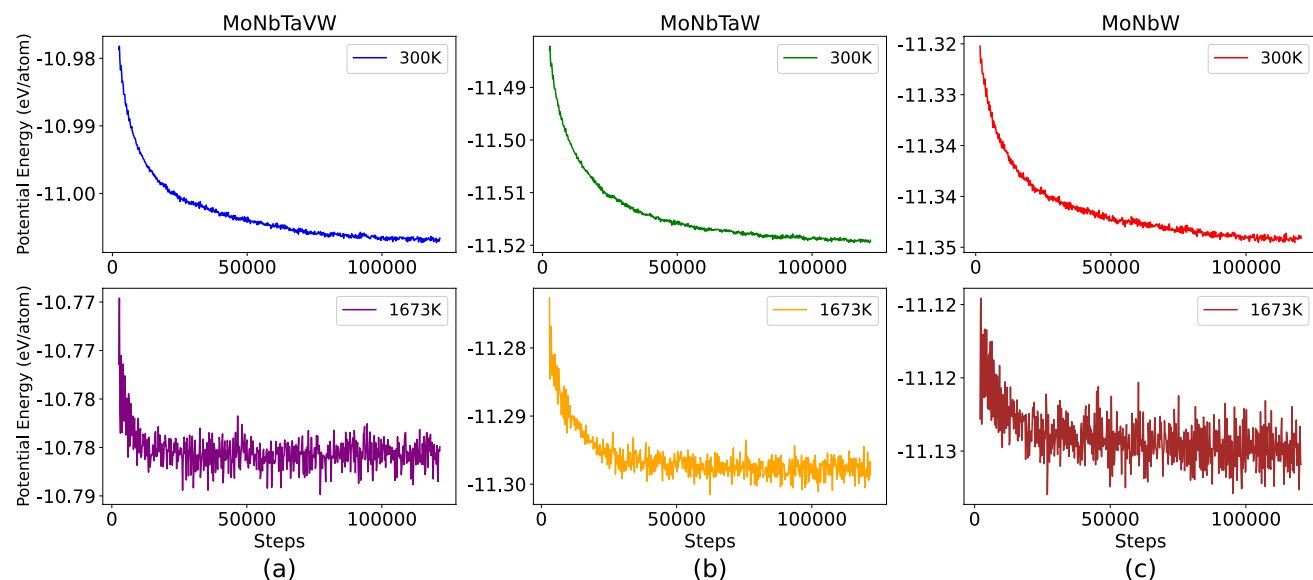


Fig. 1 Evolution of potential energy per atom during hybrid MD/MC simulations for **a** MoNbTaVW, **b** MoNbTaW, and **c** MoNbW alloy systems at 300 K (top row) and 1673 K (bottom row)

concentration of the j -type atom, and δ_{ij} is the Kronecker delta function, i.e.,

$$\delta_{ij} = \begin{cases} 1 & \text{if } i = j \\ 0 & \text{if } i \neq j \end{cases} \quad (2)$$

Lattice Distortion and Atomic Size Mismatch

To describe the lattice distortion in RMPEAs, we use the following equation [34]:

$$\Delta d = \frac{1}{N} \sum_i \sqrt{(x_i - x'_i)^2 + (y_i - y'_i)^2 + (z_i - z'_i)^2}, \quad (3)$$

where (x_i, y_i, z_i) and (x'_i, y'_i, z'_i) are the reduced coordinates of the unrelaxed and relaxed positions of atom i , respectively, while N is the total number of atoms in the system.

Atomic size mismatch Δ for a given alloy is calculated using the formula [35, 36]

$$\Delta = \sqrt{\frac{\sum c_i \Delta \bar{V}_i^2}{3V_{\text{alloy}}}}, \quad (4)$$

where $V_{\text{alloy}} = a_0^3/4$ [36], where a_0 is the lattice parameter of the alloy. In this formula, $\Delta \bar{V}_i = V_i - \bar{V}$ represents the difference between the volume of each element V_i and the average volume \bar{V} , which is given by $\bar{V} = \sum c_i V_i$.

MD Simulation for Compressive and Tensile Loading

For each alloy, five CSRO structures were then used for compressive and tensile loading simulations using MD at five different temperatures, respectively. For example, the CSRO structure annealed at 300 K was subject to a uniaxial

loading at 300 K. The same structure was not subject to loading at any other temperatures. Similarly, the CSRO structure annealed at 873 K was only subject to loading at 873 K. This simulation plan is to mimic the actual application, whereas an alloy is kept at a certain temperature for a long time.

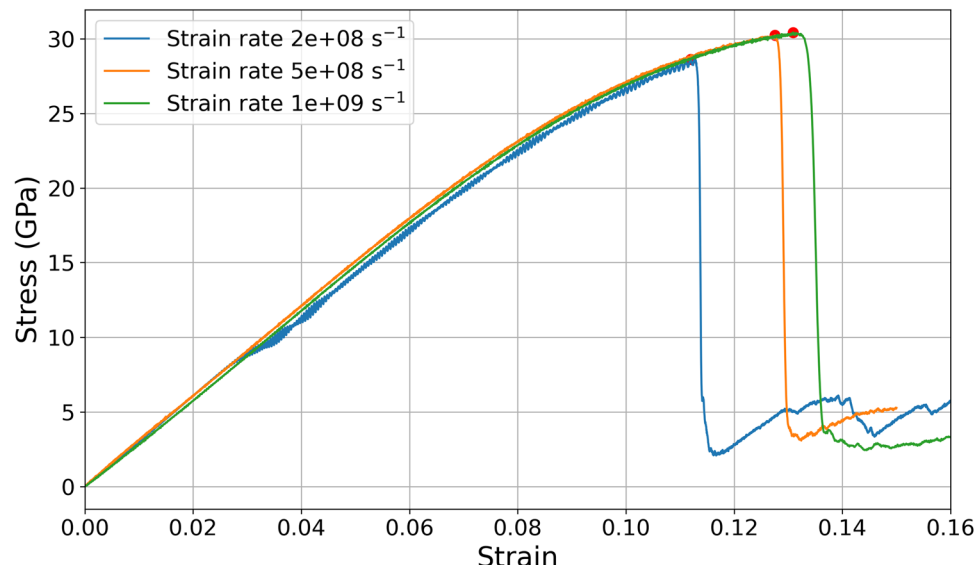
For the deformation phase, uniaxial tensile and compressive stress were applied along the z -axis. Again, PBCs were applied in all three directions. An NPT ensemble was applied to maintain the temperature at a specified constant value, while pressures in the lateral (x and y) directions were held at zero. A constant engineering strain rate of $|\dot{\epsilon}| = 5 \times 10^8 \text{ s}^{-1}$ was applied until the engineering strain reached a magnitude of ± 0.25 . Figure 2 shows that the strain rate of $5 \times 10^8 \text{ s}^{-1}$ is sufficiently low. The uniaxial engineering stress was calculated using the virial stress formulation [37].

Results and Discussion

WCP

In Fig. 3a, c, the atomic arrangements of CSRO MoNbTaVW and CSRO MoNbW alloys annealed at 300 K and 1673 K are displayed. At both temperatures, the pronounced CSRO is observed. The heatmaps in Fig. 3b, d illustrate the WCP for these alloys. In MoNbTaVW, pairs such as Mo-Ta, W-V, Mo-Nb, and Mo-Ta exhibit negative WCP values, indicating a preference for clustering. Among like atoms, the Nb-Nb pair shows positive WCP values, suggesting a tendency to cluster. In MoNbW, strong negative WCP values for Mo-Nb pairs indicate clustering, while positive WCP values for W-W pairs suggest self-pairing, which is visually confirmed in the atomic arrangement. Using the ML-based

Fig. 2 Stress-strain curves for CSRO MoNbTaVW (annealed at 300 K) under compression at 300 K at different strain rates



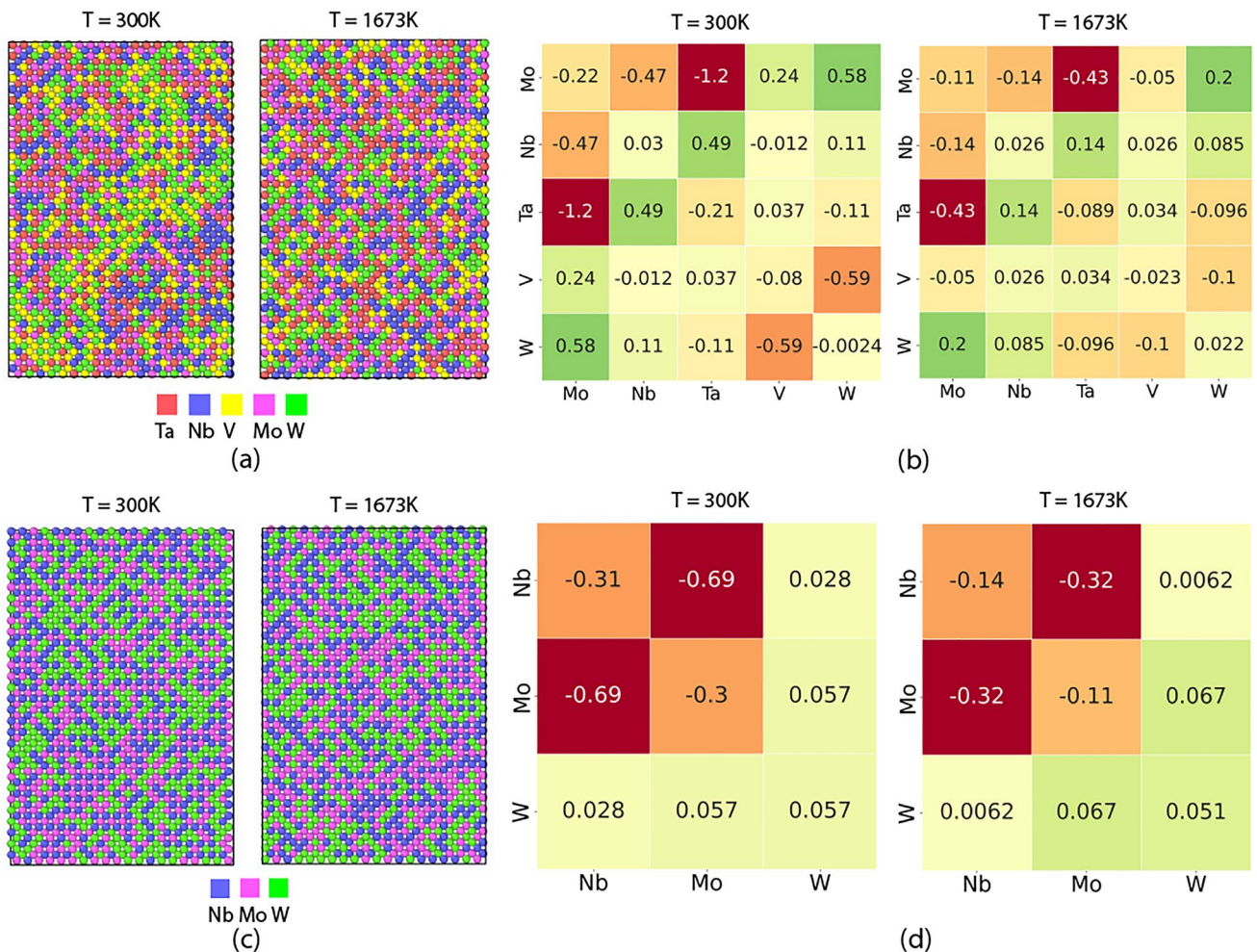


Fig. 3 Atomic arrangements of **a** MoNbTaVW and **c** MoNbW at 300 K and 1673 K, highlighting the CSRO. Corresponding heatmaps are shown in **(b)** and **(d)**

GAP, Byggmästar et al. [38] reported clustering tendencies for pairs like Mo–Ta, Mo–Nb, and W–V, which align with the observations in this study. The relatively high negative WCP of –0.43 for the Mo–Ta pair at 1673 K suggests that Mo and Ta atoms still exhibit a tendency for local clustering even at high temperatures. This observation aligns with Byggmästar et al. [38], who reported that Mo–Ta interactions retain notable ordering beyond 1000 K. The varying mixing energies among atomic pairs underscore these clustering behaviors. Moreover, our results reveal that WCP values decrease as the annealing temperature increases from 300 K to 1673 K, following trends reported in many previous studies [8, 9]. The WCP values of all 16 alloys at five different temperatures are added to Supplementary Information as Figures S1–S16.

Lattice Distortion

The lattice distortion of all 16 alloys is plotted across different temperatures in Fig. 4. The results indicate that the variation in lattice distortion with the annealing temperature is non-negligible for most alloys, except for MoTaW and NbTaW, which exhibit very small changes. The lattice distortion decreases with increasing temperature for the majority of the alloys, consistent with findings by Wang et al. [3] and Mubassira et al. [28]. Alloys such as TaVW and NbTaV show higher lattice distortion compared to others, highlighting their pronounced atomic-level strain. These trends suggest that specific alloy compositions and temperature conditions significantly influence lattice distortion.

A random forest regressor [39] was trained to predict lattice distortion based on atomic size mismatch and maximum absolute WCP values. Results for two different temperatures, 300 K and 1673 K, are presented in Fig. 5, which indicate a strong agreement between predicted and

Fig. 4 Lattice distortion across five temperatures for different alloys

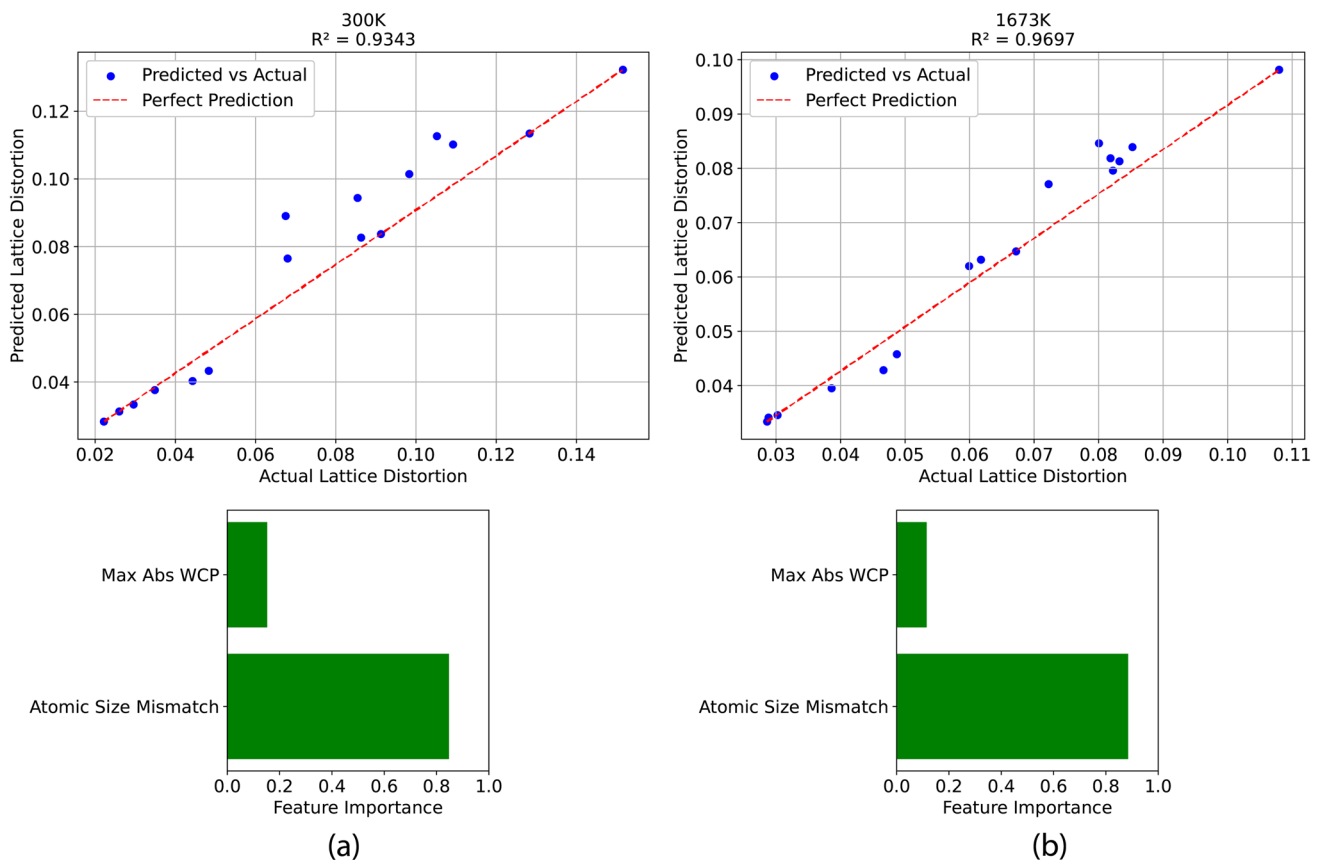
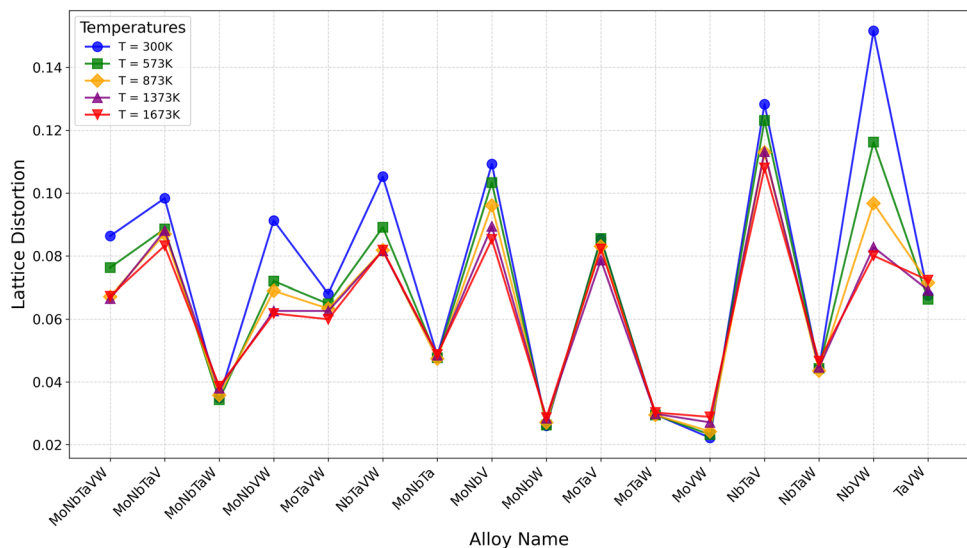


Fig. 5 Feature importance analysis shows the relative contribution of atomic size mismatch and the maximum absolute WCP in predicting lattice distortion at **a** 300 K and **b** 1673 K across 16 different alloys using random forest regressor

actual lattice distortion, as demonstrated by high R^2 values of 0.9343 and 0.9697. Feature importance analysis reveals that atomic size mismatch consistently plays a more significant

role in predicting lattice distortion than the maximum absolute WCP.

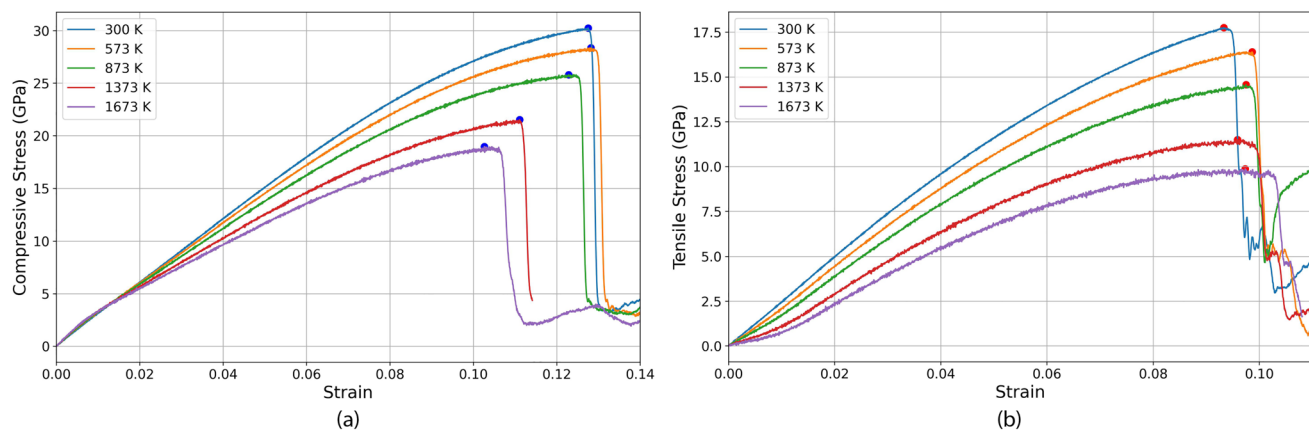


Fig. 6 **a** Compressive and **b** tensile stress–strain curves for the MoNbTaVW alloy at different temperatures. In **a** and **b**, respectively, blue and red dots mark the yield points (Color figure online)

Yield Stress

In a stress–strain curve, the yield point is identified as the point where the rate of increase in stress with respect to strain (i.e., the derivative of the stress–strain curve) is at its maximum [40, 41], as shown in Fig. 6. Across all temperatures, the compressive yield stress is consistently higher than the tensile yield stress for the same alloy, indicating that the materials can withstand higher compressive loads before yielding compared to tensile loads, as shown in Fig. 7. Another general trend is that, as the temperature increases (i.e., from 300 K to 1673 K), the yield stress (both compressive and tensile) decreases for all alloys.

We also note that there is a significant variation in yield stress among different alloys. Specifically, MoTaW and MoVW exhibit the highest yield stress values, both in compression and tension, across all tested temperatures. Alloys such as MoNbTaW, MoNbVW, MoTaVW, and MoNbW show mid-to-high-range yield stresses. MoNbTaVW, MoNbTa, MoTaV, NbTaV, and TaVW fall into the mid-range category, exhibiting moderate yield stress levels. In contrast, MoNbTaV, NbTaVW, MoNbV, and NbVW display lower mid-range yield stresses, while NbTaV consistently exhibits the lowest yield stress among all alloys studied. This stratification highlights the variation in mechanical strength across the compositions of alloys. Values of both compressive and tensile yield stresses of all alloys across all temperatures are included in Supplementary Information Table S1.

Figure 8a demonstrates that the compressive-to-tensile yield stress ratio ranges between 1.5 and 2.0. This ratio increases with temperature for all alloys (Fig. 8b). Alloys like MoNbVW, NbTaV, and NbVW have small variations in yield stress ratios across different conditions, highlighting their mechanical stability at high temperatures.

Results shown in Fig. 9 highlight the relationship between lattice distortion and yield stress ratio across

various temperatures. It confirms that a higher temperature is correlated with an elevated yield stress ratio, highlighting the influence of thermal effects on the alloys' mechanical properties. It could also be deducted that the trend is showing upward for the yield stress ratio as the lattice distortion increases.

ML Models for Yield Stress Prediction

ML models based on a random forest regressor were trained to predict the yield stresses. The random forest regressor was selected because it effectively handles high-dimensional data and captures complex relationships between features and targets [39]. With 80 data points for either compression or tension, multiple decision trees are combined to reduce overfitting and improve prediction accuracy. The models were optimized by imputing missing values using the mean strategy and standardizing the features. These missing values originated from the quaternary and ternary alloy systems, where not all WCP were available. Out of the 24 features, recursive feature elimination (RFE) was used to identify the top 20 most relevant features by iteratively removing the least important ones, and the top 10 were selected for further analysis [42]. RobustScaler was employed to standardize the features by removing the median and scaling by the interquartile range, ensuring robustness against outliers and improving model performance. Additionally, hyperparameter tuning was conducted for the ML models to optimize parameters like the number of estimators, maximum depth, and minimum samples per split, enhancing the model's predictive accuracy. The combination of RFE for feature selection, RobustScaler for handling outliers, and hyperparameter tuning collectively contributed to improved performance by ensuring the model focused on relevant features and processed data effectively.

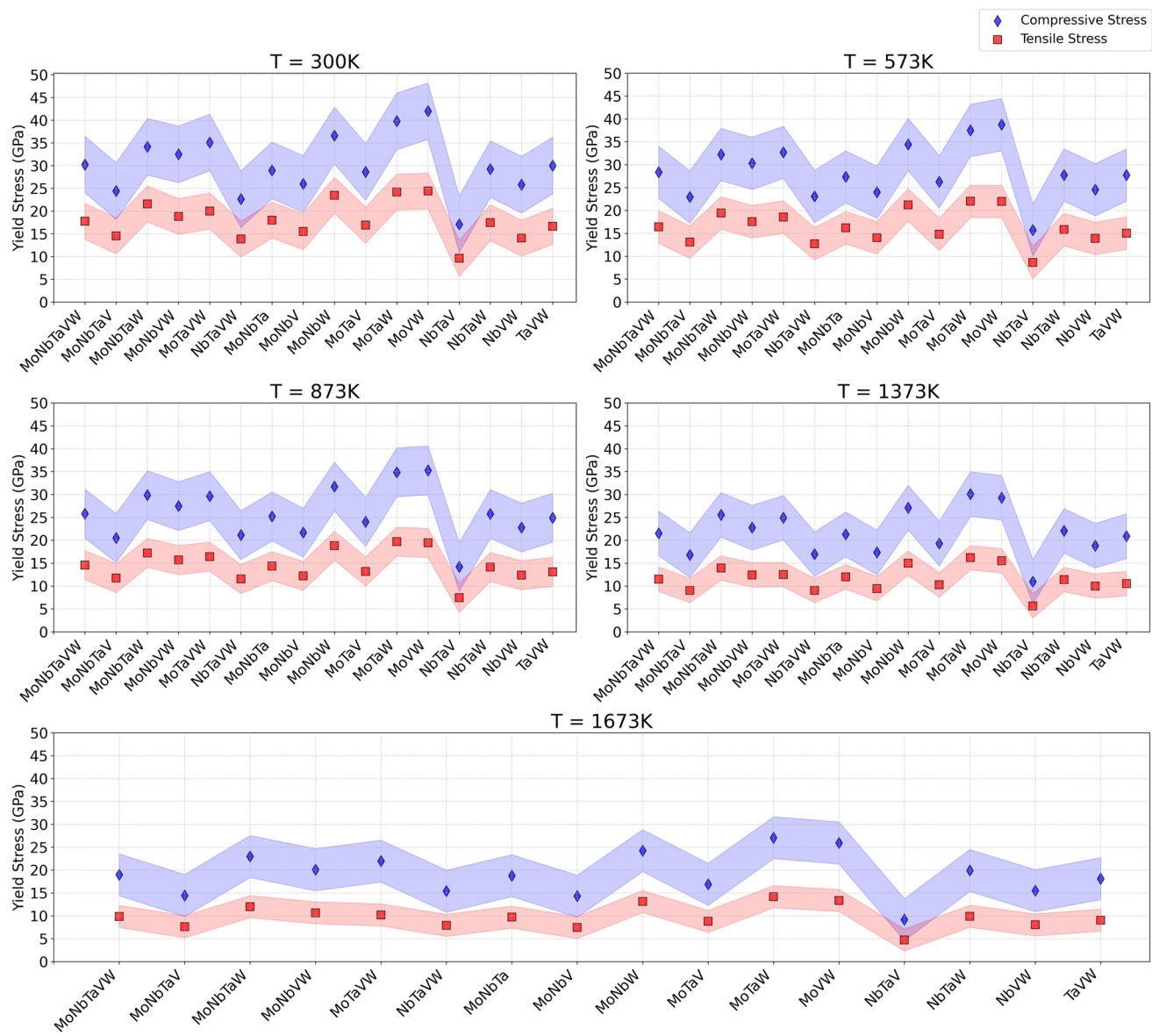


Fig. 7 Compressive and tensile yield stresses of the CSRO structures at five temperatures for 16 alloys. The shaded blue/red regions are only for visualization purposes to highlight that the compressive

yield stresses are generally above the tensile yield stress. The shaded regions do not have any underlying mathematical or physical implications (Color figure online)

Results demonstrate that lattice distortion and temperature are consistently the most influential features in predicting mechanical properties. For the compressive yield stress (Fig. 10a), lattice distortion is the most important feature, followed by temperature and WCP values of the Ta-Ta pair, with the model achieving an excellent R^2 score of 0.96. Similarly, for the tensile yield stress (Fig. 10b), lattice distortion and temperature remain the key factors, along with WCP values of the Ta-Ta pair and the Mo concentration, yielding an even higher R^2 score of 0.97. In predicting the yield stress ratio (Fig. 10c), temperature surpasses lattice distortion to become the most important feature, highlighting the thermal dependency of this

ratio, with the model achieving a solid R^2 score of 0.88. WCP values of pairs, such as Ta-Ta, Nb-Ta, and W-W, also significantly influence the ratio, suggesting that atomic-level clustering plays a critical role in plastic anisotropy.

Conclusion

This study examines the plastic anisotropy in 16 RMPEAs, the underlying atomic interactions influencing this anisotropy, and the effects of temperature using a combination

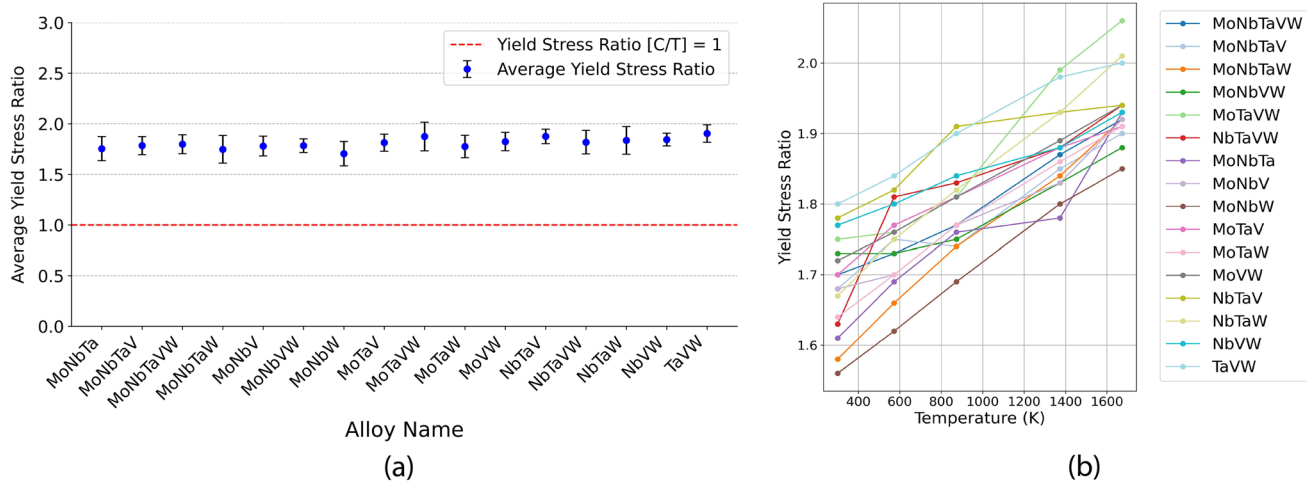
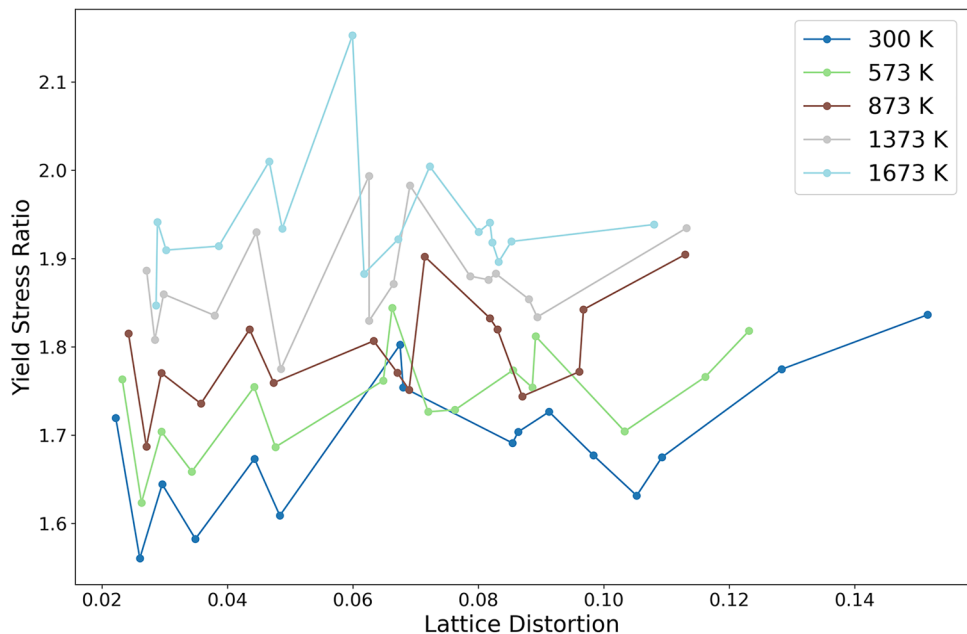


Fig. 8 **a** Average yield stress ratio (compressive to tensile) for 16 alloys. Error bars represent the standard deviation among five temperatures. The red dashed line at a ratio of 1 indicates where the com-

pressive and tensile yield stresses are equal. **b** The yield stress ratio across five temperatures (Color figure online)

Fig. 9 The variation of yield stress ratio with lattice distortion across different temperatures



of atomistic simulations and ML approaches. The analysis reveals that the compressive yield stress is consistently higher than the tensile yield stress across all temperatures, and both decrease with an increasing temperature, highlighting the alloys' temperature-dependent mechanical behavior. Alloys such as MoTaW and MoVW exhibit the highest yield stress values, while NbTaV consistently shows the lowest, underscoring the significant variation in

mechanical strength among different compositions. Lattice distortion and temperature emerge as critical factors influencing mechanical properties, with ML models achieving high predictive accuracy by leveraging these quantities alongside WCP for specific atomic pairs.

The study also identifies pronounced CSRO in the atomic arrangements, with clustering tendencies between the same two species influenced by the constituent elements. WCP

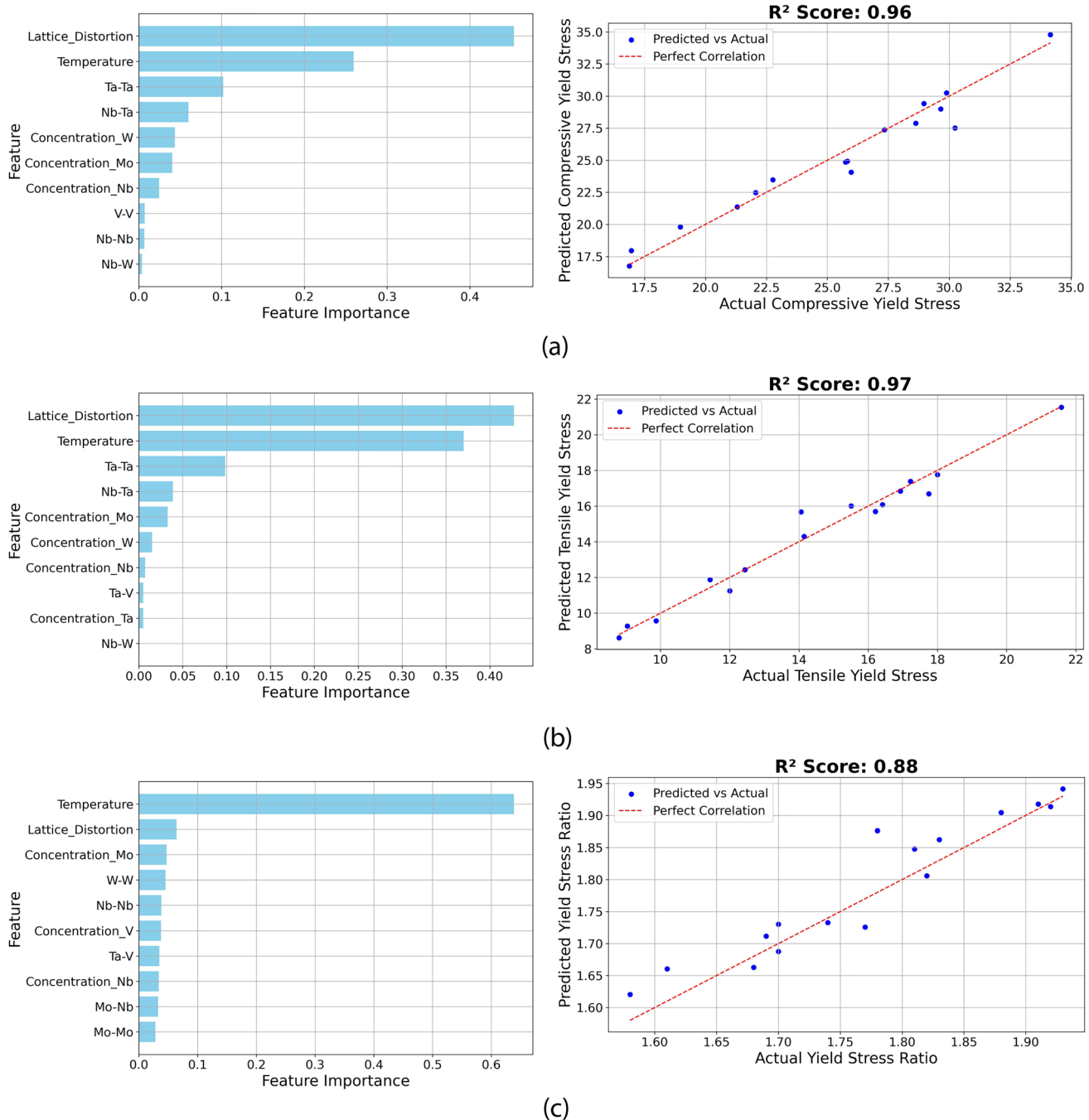


Fig. 10 R^2 plot and top 10 important features for predicting **a** compressive yield stress, **b** tensile yield stress, and **c** compressive-to-tensile yield stress ratio

values decrease with the annealing temperature, suggesting reduced atomic ordering at higher temperatures, consistent with trends reported in the previous studies. Additionally, ML models reveal that temperature and lattice distortion are the most significant features for predicting compressive and tensile yield stress, along with the WCP value of Ta-Ta pair

and the concentration of Mo. These findings highlight the critical role of atomic-scale interactions, lattice distortion, and temperature in determining the mechanical behavior of RMPEAs, offering valuable insights for designing alloys with tailored properties for high-temperature applications.

Supplementary Information The online version contains supplementary material available at <https://doi.org/10.1007/s44210-025-00054-6>.

Author Contributions YS designed and supervised the project. AAM performed atomistic simulations and built machine learning models with input from SX and XL. AAM prepared the original draft. XL, SX, and YS revised the draft. All authors read and approved the final manuscript.

Funding This work used Bridges-2 at the Pittsburgh Supercomputing Center through allocation MAT220034 from the Advanced Cyberinfrastructure Coordination Ecosystem: Services & Support (ACCESS) program, which is supported by National Science Foundation Grants #2138259, #2138286, #2138307, #2137603, and #2138296. The support and resources from the Center for High Performance Computing at the University of Utah are gratefully acknowledged. AAM and YS thank the start-up funds provided by the Utah State University.

Data Availability The datasets generated and/or analyzed during the current study are available from the corresponding author upon reasonable request.

Declarations

Conflict of interest The authors declare that they have no Conflict of interest, including personal, professional, financial, or any other type.

Ethical Approval Not applicable.

Consent to Participate Not applicable.

Consent to Publish Not applicable.

Open Access This article is licensed under a Creative Commons Attribution 4.0 International License, which permits use, sharing, adaptation, distribution and reproduction in any medium or format, as long as you give appropriate credit to the original author(s) and the source, provide a link to the Creative Commons licence, and indicate if changes were made. The images or other third party material in this article are included in the article's Creative Commons licence, unless indicated otherwise in a credit line to the material. If material is not included in the article's Creative Commons licence and your intended use is not permitted by statutory regulation or exceeds the permitted use, you will need to obtain permission directly from the copyright holder. To view a copy of this licence, visit <http://creativecommons.org/licenses/by/4.0/>.

References

- O.N. Senkov, G.B. Wilks, D.B. Miracle, C.P. Chuang, P.K. Liaw, Refractory high-entropy alloys. *Intermetallics* **18**(9), 1758–1765 (2010)
- O.N. Senkov, G.B. Wilks, J.M. Scott, D.B. Miracle, Mechanical properties of Nb₂₅Mo₂₅Ta₂₅W₂₅ and V₂₀Nb₂₀Mo₂₀Ta₂₀W₂₀ refractory high entropy alloys. *Intermetallics* **19**(5), 698–706 (2011)
- T. Wang, J. Li, M. Wang, C. Li, Y. Su, S. Xu, X.-G. Li, Unraveling dislocation-based strengthening in refractory multi-principal element alloys. *NPJ Comput. Mater.* **10**(1), 143 (2024)
- R.K. Nutor, Q. Cao, X. Wang, D. Zhang, Y. Fang, Y. Zhang, J.-Z. Jiang, Phase selection, lattice distortions, and mechanical properties in high-entropy alloys. *Adv. Eng. Mater.* **22**(11), 2000466 (2020)
- Q. He, Y. Yang, On lattice distortion in high entropy alloys. *Front. Mater.* **5**, 42 (2018)
- C. Lee, G. Song, M.C. Gao, R. Feng, P. Chen, J. Brechtl, Y. Chen, K. An, W. Guo, J.D. Poplawsky et al., Lattice distortion in a strong and ductile refractory high-entropy alloy. *Acta Materialia* **160**, 158–172 (2018)
- S. Mubassira, W.-R. Jian, S. Xu, Effects of chemical short-range order and temperature on basic structure parameters and stacking fault energies in multi-principal element alloys. *Modelling* **5**(1), 352–366 (2024)
- H. Zheng, L.T. Fey, X.-G. Li, Y.-J. Hu, L. Qi, C. Chen, S. Xu, I.J. Beyerlein, S.P. Ong, Multi-scale investigation of short-range order and dislocation glide in monbti and tanbti multi-principal element alloys. *NPJ Comput. Mater.* **9**(1), 89 (2023)
- S. Xu, W.-R. Jian, I.J. Beyerlein, Ideal simple shear strengths of two HfNbTaTi-based quinary refractory multi-principal element alloys. *APL Mater.* **10**(11), 111107 (2022)
- S. Chen, Z.H. Aitken, S. Pattamatta, Z. Wu, Z.G. Yu, D.J. Srolovitz, P.K. Liaw, Y.-W. Zhang, Short-range ordering alters the dislocation nucleation and propagation in refractory high-entropy alloys. *Mater. Today* **65**, 14–25 (2023)
- S. Yin, Y. Zuo, A. Abu-Odeh, H. Zheng, X.-G. Li, J. Ding, S.P. Ong, M. Asta, R.O. Ritchie, Atomistic simulations of dislocation mobility in refractory high-entropy alloys and the effect of chemical short-range order. *Nat. Commun.* **12**(1), 4873 (2021)
- D. Patel, M.D. Richardson, B. Jim, S. Akhmadaliev, R. Goodall, A.S. Gandy, Radiation damage tolerance of a novel metastable refractory high entropy alloy V_{2.5}Cr_{1.2}WMoCo_{0.04}. *J. Nucl. Mater.* **531**, 152005 (2020)
- O. El-Atwani, N. Li, M. Li, A. Devaraj, J.K.S. Baldwin, M.M. Schneider, D. Sobieraj, J.S. Wróbel, D. Nguyen-Manh, S.A. Maloy et al., Outstanding radiation resistance of tungsten-based high-entropy alloys. *Sci. Adv.* **5**(3), 2002 (2019)
- S. Zhao, Defect properties in a VTaCrW equiatomic high entropy alloy (HEA) with the body centered cubic (bcc) structure. *J. Mater. Sci. Technol.* **44**, 133–139 (2020)
- J.-P. Couzinié, O. Senkov, D. Miracle, G. Dirras, Comprehensive data compilation on the mechanical properties of refractory high-entropy alloys. *Data in Brief* **21**, 1622–1641 (2018)
- F.G. Coury, M. Kaufman, A.J. Clarke, Solid-solution strengthening in refractory high entropy alloys. *Acta Materialia* **175**, 66–81 (2019)
- W. Huang, X. Wang, J. Qiao, Y. Wu, Microstructures and mechanical properties of TiZrHfNbTaW_x refractory high entropy alloys. *J. Alloys Compd.* **914**, 165187 (2022)
- O.N. Senkov, S. Gorsse, D.B. Miracle, High temperature strength of refractory complex concentrated alloys. *Acta Materialia* **175**, 394–405 (2019)
- Q. Peng, F. Meng, Y. Yang, C. Lu, H. Deng, L. Wang, S. De, F. Gao, Shockwave generates (100) dislocation loops in bcc iron. *Nat. Commun.* **9**(1), 4880 (2018)
- W.-L. Hsu, C.-W. Tsai, A.-C. Yeh, J.-W. Yeh, Clarifying the four core effects of high-entropy materials. *Nat. Rev. Chem.* **8**, 471–485 (2024)
- S. Xu, A. Al Mamun, S. Mu, Y. Su, Uniaxial deformation of nanowires in 16 refractory multi-principal element alloys. *J. Alloys Compd.* **959**, 170556 (2023)
- S.Z. Chavoshi, S. Xu, S. Goel, Addressing the discrepancy of finding the equilibrium melting point of silicon using molecular dynamics simulations. *Proc. R. Soc. A* **473**(2202), 20170084 (2017)
- J. Li, Q. Fang, B. Liu, Y. Liu, Y. Liu, Mechanical behaviors of alcrfecuni high-entropy alloys under uniaxial tension via molecular dynamics simulation. *RSC Adv.* **6**(80), 76409–76419 (2016)

24. Y. Qi, M. Zhao, M. Feng, Molecular simulation of microstructure evolution and plastic deformation of nanocrystalline co-cfemnni high-entropy alloy under tension and compression. *J. Alloys Compd.* **851**, 156923 (2021)
25. A. Al Mamun, S. Xu, X.-G. Li, Y. Su, Comparing interatomic potentials in calculating basic structural parameters and Peierls stress in tungsten-based random binary alloys. *Physica Scripta* **98**(10), 105923 (2023)
26. Y. Zuo, C. Chen, X. Li, Z. Deng, Y. Chen, J. Behler, G. Csányi, A.V. Shapeev, A.P. Thompson, M.A. Wood et al., Performance and cost assessment of machine learning interatomic potentials. *J. Phys. Chem. A* **124**(4), 731–745 (2020)
27. J. Byggmästar, A. Hamedani, K. Nordlund, F. Djurabekova, Machine-learning interatomic potential for radiation damage and defects in tungsten. *Phys. Rev. B* **100**(14), 144105 (2019)
28. S. Mubassira, M. Fani, A. Raj, C. Hirt, R.S. Brinlee, A. Poozesh, W.-R. Jian, S.Z. Chavoshi, C. Lee, S. Xu, Chemical short-range order and its influence on selected properties of non-dilute random alloys. *Comput. Mater. Sci.* **248**, 113587 (2025)
29. Y. Pan, T. Fu, M. Duan, C. Li, H. Hu, X. Peng, Tension-compression asymmetry of BCC NbMoTaW in high entropy alloy nanowires. *ACS Appl. Nano Mater.* **7**(7), 8121–8129 (2024)
30. A.V. Shapeev, Moment tensor potentials: a class of systematically improvable interatomic potentials. *Multiscale Model. Simul.* **14**(3), 1153–1173 (2016)
31. A.P. Thompson, H.M. Aktulg̃a, R. Berger, D.S. Bolintineanu, W.M. Brown, P.S. Crozier, P.J. Veld, A. Kohlmeyer, S.G. Moore, T.D. Nguyen, R. Shan, M.J. Stevens, J. Tranchida, C. Trott, S.J. Plimpton, LAMMPS - a flexible simulation tool for particle-based materials modeling at the atomic, meso, and continuum scales. *Comp. Phys. Comm.* **271**, 108171 (2022)
32. J.M. Cowley, An approximate theory of order in alloys. *Phys. Rev.* **77**(5), 669 (1950)
33. D. Fontaine, The number of independent pair-correlation functions in multicomponent systems. *J. Appl. Crystallogr.* **4**(1), 15–19 (1971)
34. H. Song, F. Tian, Q.-M. Hu, L. Vitos, Y. Wang, J. Shen, N. Chen, Local lattice distortion in high-entropy alloys. *Phys. Rev. Mater.* **1**(2), 023404 (2017)
35. C. Varvenne, A. Luque, W.A. Curtin, Theory of strengthening in fcc high entropy alloys. *Acta Materialia* **118**, 164–176 (2016)
36. A. Esfandiarpour, R. Alvarez-Donado, S. Papanikolaou, M. Alava, Atomistic simulations of dislocation plasticity in concentrated VCoNi medium entropy alloys: effects of lattice distortion and short range order. *Front. Mater.* **9**, 1046291 (2022)
37. T. Trusty, S. Xu, I.J. Beyerlein, Atomistic simulations of tungsten nanotubes under uniform tensile loading. *J. Appl. Phys.* **126**(9), 095105 (2019)
38. J. Byggmästar, K. Nordlund, F. Djurabekova, Modeling refractory high-entropy alloys with efficient machine-learned interatomic potentials: defects and segregation. *Phys. Rev. B* **104**(10), 104101 (2021)
39. Q. Wang, T.-T. Nguyen, J.Z. Huang, T.T. Nguyen, An efficient random forests algorithm for high dimensional data classification. *Adv. Data Anal. Classif.* **12**, 953–972 (2018)
40. S. Xu, Modelling plastic deformation of nano/submicron-sized tungsten pillars under compression: a coarse-grained atomistic approach. *Int. J. Multiscale Comput. Eng.* **16**(4), 367–376 (2018)
41. S. Xu, M.I. Latypov, Y. Su, Concurrent atomistic-continuum simulations of uniaxial compression of gold nano/submicropillars. *Philos. Mag. Lett.* **98**(5), 173–182 (2018)
42. I. Guyon, J. Weston, S. Barnhill, V. Vapnik, Gene selection for cancer classification using support vector machines. *Mach. Learn.* **46**(1), 389–422 (2002)

Publisher's Note Springer Nature remains neutral with regard to jurisdictional claims in published maps and institutional affiliations.